Paper VII-1 presented at the 1st International Workshop on Progress in Nb-based Superconductors, National Institute for Materials Science, Tsukuba, Japan, Feb. 2-3, 2004. Published in "Progress of Nb-based Superconductors: Proceedings of International Workshop on Nb-Based Superconductors," Ed. K Inoue, T. Takeuchi and A. Kikuchi, pub. Maeda printing Co. Ltd., Japan, pp. 1-8, 2005."

Microstructural and Microchemical Homogeneity for High Critical Current Density in Nb_3Sn

P. J. Lee and D. C. Larbalestier

The Applied Superconductivity Center, The University of Wisconsin-Madison
Madison, WI 53706-1609, USA

Abstract

High critical current density Nb_3Sn strands developed for high field accelerator magnets achieve layer critical current densities exceeding 3000 A/mm^2 at 12 T (4.2 K). Strand of this type has been used by the Supercon group at LBNL to successfully fabricate a 16 T (4.2 K) dipole accelerator magnet. These strands have remarkably uniform microstructures and chemistry compared with earlier generations of Nb_3Sn. The grain size of this strand has been measured across the A15 layer and was found to be small (110 nm diameter) but not much smaller than much lower J_c strands, however the Nb_3Sn grains are very homogeneous in morphology and size. This is despite an A15 layer thickness of 10 to 20 μm. We show how high resolution FESEM can be used to reveal microstructural and microchemical variations in both high critical current density Nb-Ti and Nb_3Sn and draw parallels between the two.

Introduction

The Nb based superconductors Nb-Ti and Nb_3Sn are the dominant commercial superconductors with well established industries for production and application. These two superconductors, however, are rarely compared in the same publications so we take the opportunity of the 1st International Workshop on Progress of Nb-based Superconductors to review some of the similarities that have emerged between Nb_3Sn and Nb-Ti, particularly in microstructural and microchemical homogeneity, and look to the future of their development.

Much of the development of Nb-Ti as a large scale high performance superconductor took place prior to 1990. Nb-Ti had been just one of a number of superconducting transition metal alloys investigated by Hulm and Blaugher (1961)[1], including Nb-Zr which successfully competed with Nb-Ti into the 1970s. Coincidentally 1961 also saw the breakthrough powder-in-tube Nb_3Sn conductor of Kunzler et al. [2] which for the first time demonstrated high field superconductivity (~10^3 A/mm^2 at magnetic fields as large as 8.8 T). Kunzler et al.'s conductor had to be heat treated at high temperature (970 °C - 1400 °C) but it was clear from their work that lower temperatures produced far higher critical current densities. For a Nb-Sn diffusion couple, however, temperatures had to exceed 930 ºC in order to produce only the superconducting A15 phase at the interface. In the 1970s the first A15 compounds were produced by the bronze process [3,4,5] and, like the subsequent internal Sn process, the presence of Cu [6] allowed the production of the A15 phase at low temperatures (>600 °C). Low temperature resulted in a fine A15 grain size and thus a high density of grain boundaries, which, being the primary flux-pinning center, produced high critical current densities.

By 1983 Nb-Ti based strand had been used on a very large scale in the FNAL Tevatron, establishing a mature industry that would come to be dominated by MRI production. By that time it was understood that heat treatment of the Nb-Ti at intervals during the wire drawing process greatly increased the critical current density, moving far beyond that available with NbZr. By 1984 the Baoji group had achieved 3400 A/mm² (5 T, 4.2 K) through multiple heat

treatment and drawing cycles [7], a level that exceeds most commercial Nb-Ti today. Further improvements in conventional heat treated Nb-Ti have been relatively small, with the highest reported values, ~4000 A/mm² at 5 T, 4.2 K, requiring extensive heat treatments[8]. Using the Artificial Pinning Center, APC, approach, the critical current density of Nb-Ti has recently been raised to 5070 A/mm² (5 T, 4.2 K) using a combination 8Ni4Cu pinning center in a Nb-47wt%Ti matrix [9]. In contrast, the increases in Nb_3Sn critical current density over the past 5 years has been quite dramatic with a two-fold increase in the actual layer critical current density of the Nb_3Sn being observed between strand development of the ITER Central Solenoid Model Coil (CSMC) and strand developed to the next generation of high energy physics accelerator magnets[10].

In this paper we take the opportunity of the 1st Workshop on Progress in Nb-based Superconductors bring to compare the microstructural and microchemical development of high critical current density Nb-Ti with the new generation of Nb_3Sn strands that have been produced in the past 5 years.

Experimental Technique

In this paper we examine a wide variety of commercially fabricated Nb-Ti and Nb_3Sn strands using high-resolution field emission scanning electron microscopy (FESEM). This enables us to compare the microstructures of these dissimilar materials under similar operating conditions. In particular atomic number sensitive backscattered electron imaging (BEI) is used to reveal compositional variations with sub 50 nm resolution [11].

Diffusion and Grain Boundaries

Because Nb_3Sn is brittle it must be formed at final wire size by the diffusion of Sn, into Nb, the most common situation (bronze process and internal Sn) being a diffusion couple of Nb-Nb_3Sn-(Cu-Sn). Nb-47Ti, however, is remarkably ductile and the filaments that will eventually be drawn to the micron level will start as 330 mm diameter billets. In order to produce high critical current densities, however, α-Ti precipitates are introduced into the Nb-Ti as pinning centers by precipitation heat treatment. For both the precipitation of α-Ti and the formation of Nb_3Sn [e.g.12,13] grain boundary diffusion dominates over bulk diffusion.

In Figs. 1 and 2 we compare atomic number sensitive BEI images taken during the heat treatment and strain cycle processing of a Nb-Ti(Fe) strand (in this case part of the strand development for the LHC IR quadrupoles)[14]. After the 1st heat treatment (Fig. 1) there is

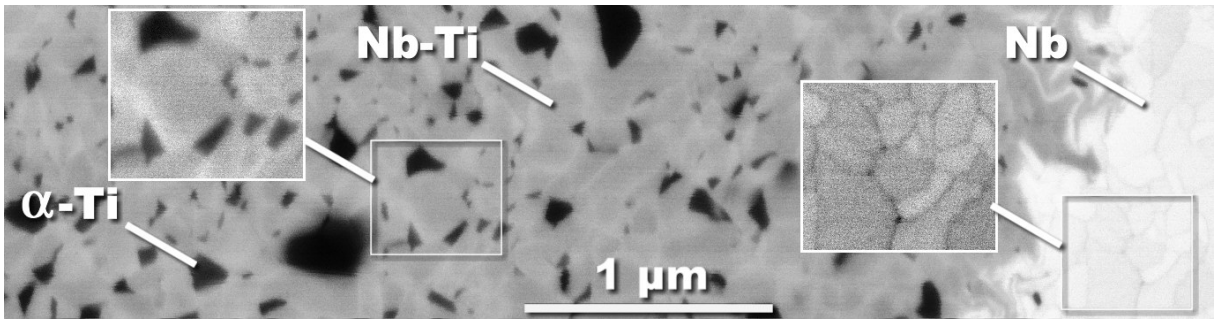

Fig. 1. BEI (atomic number sensitive) image of a partial Nb-47Ti(Fe) filament cross-section after 1 precipitation heat treatment of 80 hrs at 420 °C. The magnified inserts have had their contrast modified in order to better show the light (higher atomic number) grain boundary regions in the Nb-Ti and the dark (lower atomic number) contrast regions in the Nb diffusion barrier.

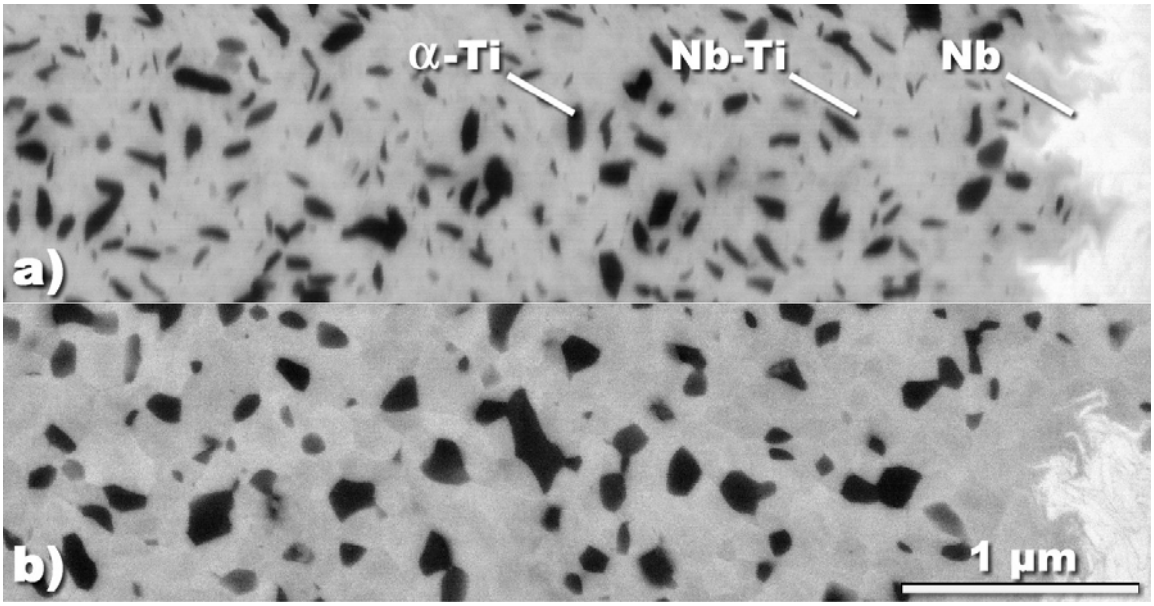

Fig. 3. BEI (atomic number sensitive) images of Nb-47Ti(Fe) filament cross-sections after a) two precipitation heat treatment followed by a cold drawing strain of 1 and b) after 2 heat treatments of 80 hrs at 420 °C and a final heat treatment of 160 hrs at 405 °C.

very strong contrast from the regions adjacent to the grain boundaries. In the Nb-Ti the regions close to the grain boundaries are light in contrast and in the Nb diffusion barrier there is a dark contrast (possibly the Cu diffusing inwards [15] or Ti outwards). The light contrast is consistent with Ti depletion of those regions, which increases the mean atomic number. This is consistent with Nb-rich regions observed by field ion microprobe [16]. As the Ti diffuses to the α-Ti precipitates (located at grain boundary triple points) much faster than through the bulk, the regions adjacent to the grain boundaries become Ti poor until no further precipitation occurs. Typically no more that 10 percent of filament volume is precipitate at this point, compared to 20 volume percent required to exceed 3000 A/mm² (5 T, 4.2 K)[17].

The microstructure must be mechanically mixed and refined by cold work strain in order for further precipitate growth to occur. This mixing is illustrated in Fig. 2a with the plane strain deformation producing a rapid inter-curling of the Nb grains. After mixing, additional Ti diffusion and precipitation occurs so that the amount of precipitate produced after three identical heat treatments is three times that from just one of those heat treatments. The implication of these microstructures, however, is that the composition of the Nb-Ti matrix is

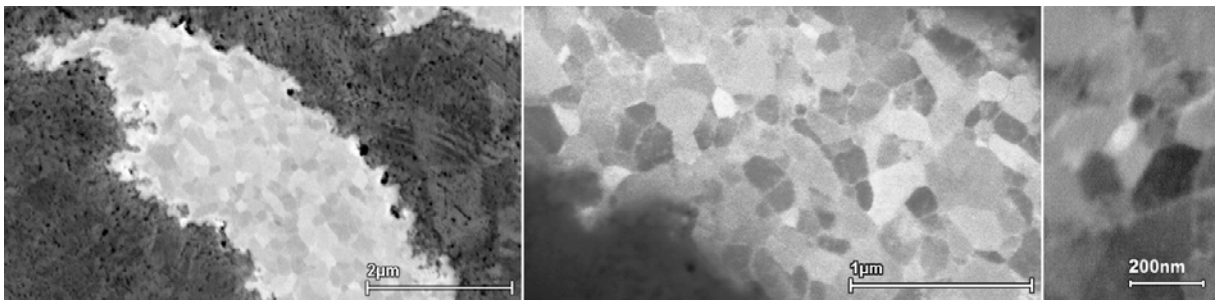

Fig. 2. BEI (atomic number sensitive) images at successively higher magnification of Nb filaments in a high field bronze (VAC NSTT) strand prior to Nb_3Sn heat treatment supplied by Manfred Thoener of VAC (now European Advanced Superconductors). Note the light contrast of the grain boundaries in the unreacted Nb compared to the dark contrast in the grain boundaries in Fig.. 1.

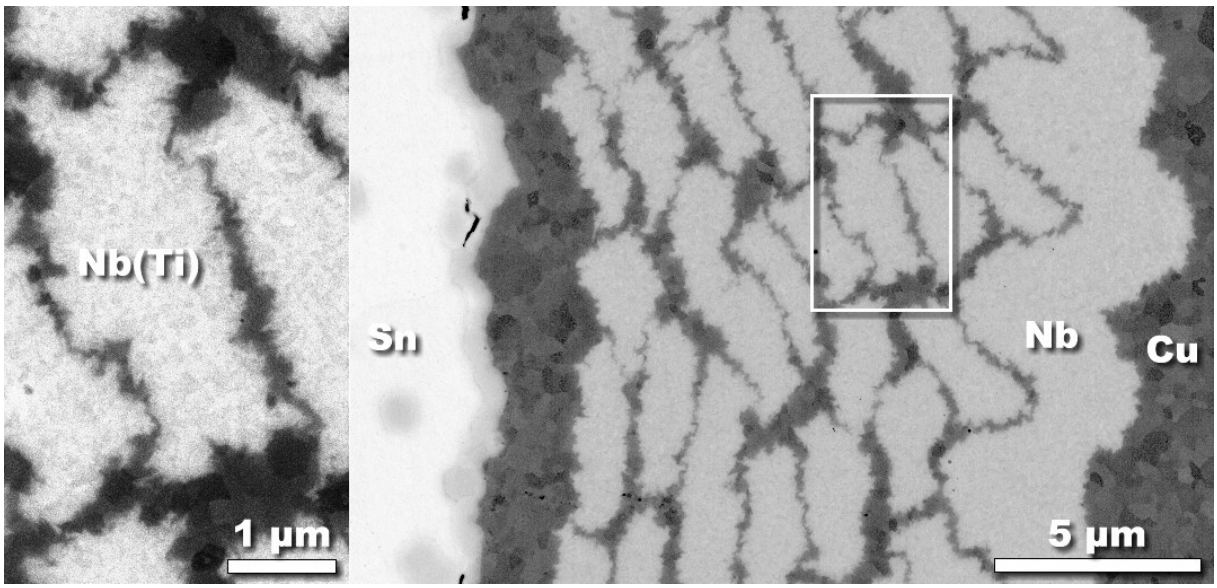

Fig. 4. BEI (atomic number sensitive) images of Nb(Ti) filaments in a high Sn MJR strand manufactured by OI-ST prior to Nb_3Sn heat treatment. The same plane strain imposed intercurling of the Nb(Ti) with the Cu matrix results in a mechanically mixed Cu and Nb interfaces and an intermediate backscatter contrast.

inhomogeneous after precipitation, even to some extent after final heat treatment and that the final drawing strain to wire size not only refines the precipitate size but also mechanically mixes the matrix Nb-Ti (the distance scale of the grain boundary Ti depletion is already much smaller ~10 nm at final heat treatment compared with 120-200 nm diameter for the α-Ti ribbons).

In the Nb barrier around the Nb-47Ti filaments in Figs. 1 and 2 the grain boundaries are dark in contrast in contrast to the unreacted Nb filaments in a bronze route Nb_3Sn composite shown in Fig. 3, which shows a light contrast. Here there is the strong suggestion from the light contrast in the grain boundaries, that Sn is being diffused into the unreacted Nb filament during the multiple anneals that are necessary to draw the bronze process strand to final size.

In Fig. 4, which shows partial cross-sections from an unreacted MJR (Modified Jelly Roll) strand at final size, we observe, at the interface between the Nb(Ti) filaments and the Cu matrix, the same plane strain imposed BCC inter-curling as seen in Nb-47Ti (Figs. 1 and 2). This results in the Nb(Ti) gains at the surface of the filaments mechanically mixing with the relatively soft adjacent Cu (producing an intermediate BEI contrast in these images). Thus the initial reaction interface is one between the Cu(Sn) and an interface of mechanically mixed Cu and Nb. Another feature clearly observable in this low-Cu high critical current density Nb_3Sn composite is the interlocking of the filaments, with often only small intermixed Cu-Nb regions separating the filaments. As will be observed later, however, the apparently obstructed diffusion path from the central Sn core to the outer filaments does not produce markedly Sn-poor outer filaments.

In Fig. 5 we show BEI images of an ITER-CSMC low hysteresis loss (high Cu) MJR internal $Nb(Ti)_3Sn(Mg)$ strand cross-section manufacture by TWC (final HT 256 hrs at 750 °C). Here the grain contrast is light (higher atomic number) for the Nb_3Sn and darker (lower atomic number) for the $Nb(Ta)_3Sn$ formed from the Nb-44 At. % Ta alloy barrier. Cu enrichment of the grain boundaries has been established as far back as 1983 by Suenaga and co-workers [18], who found both Sn and Cu enrichment at grain boundaries using a scanning

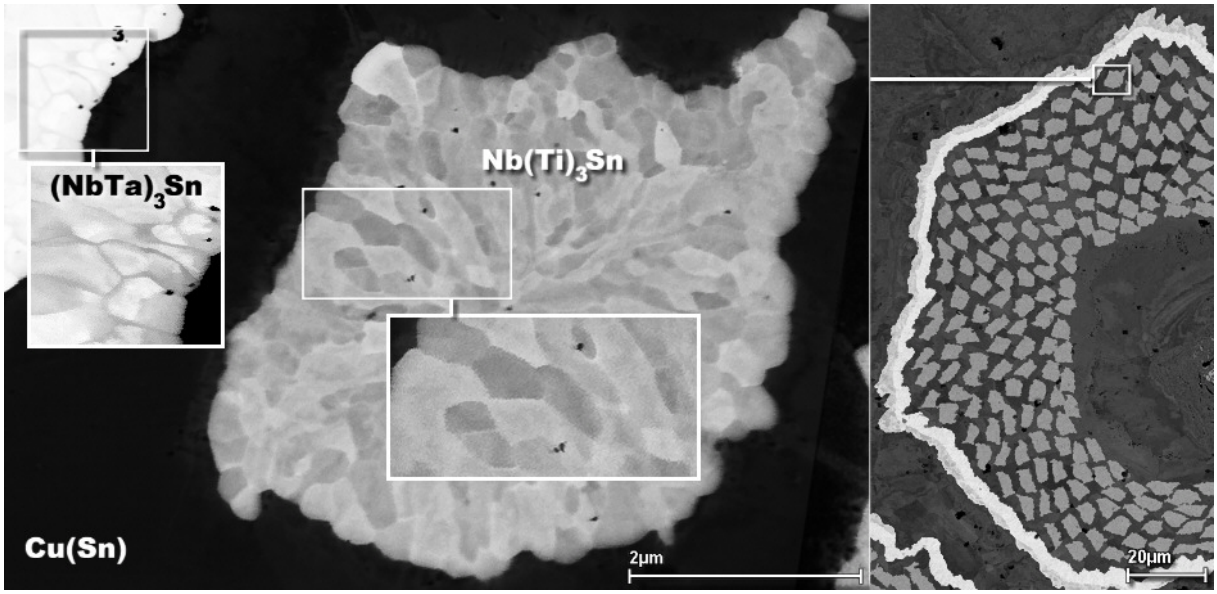

Fig. 5. BEI (atomic number sensitive) images of an ITER-CSMC generation MJR internal $Nb(Ti)_3Sn$(Mg) strand cross-section manufactured by TWC (final HT 256 hrs at 750 °C). Boxes show location of adjacent inset magnified images.

Auger microprobe. Cu has a significantly lower atomic number than Nb_3Sn, as can be seen the surrounding matrix, so this does not alone explain the uniformly increased back-scattering from the grain boundaries. More intriguing still is the image in Fig. 6 which shows a sub-element containing Nb-Ta fins manufactured for Supergenics (heat treated by E. Barzi at FNAL). The fins are designed to separate the sub-element into two semi-cylindrical filaments, thus reducing the effective filament diameter [19]. In the Nb_3Sn the grain boundary contrast changes from neutral to light as the fin is approached. In the fin the dark grain boundaries in the reacted areas increase in thickness as the Nb_3Sn is approached. In the Nb diffusion barrier (see magnified inset) light contrast in the grain boundary extends 1 μm into the barrier from the fin-Nb interface where there are discontinuous islands of Nb_3Sn less than 100 nm in diameter. This suggests the same contrast mechanism as in Fig. 3 with Sn starting to diffuse

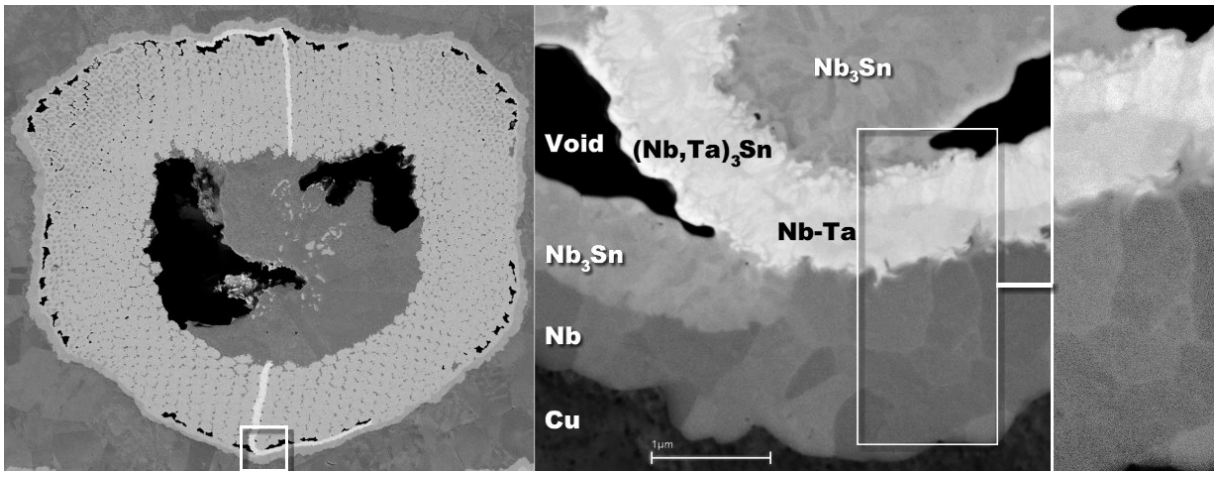

Fig. 6. BEI images of a sub-element containing Nb-Ta fins manufactured for Supergenics (final HT 20 hrs at 700 °C). In the Nb_3Sn the grain boundary contrast changes from neutral to light as the fin is approached. In the fin the dark grain boundaries in the reacted areas increase in thickness as the Nb_3Sn is approached. In the Nb diffusion barrier light contrast in the grain boundary extends 1 μm into the barrier from the fin.

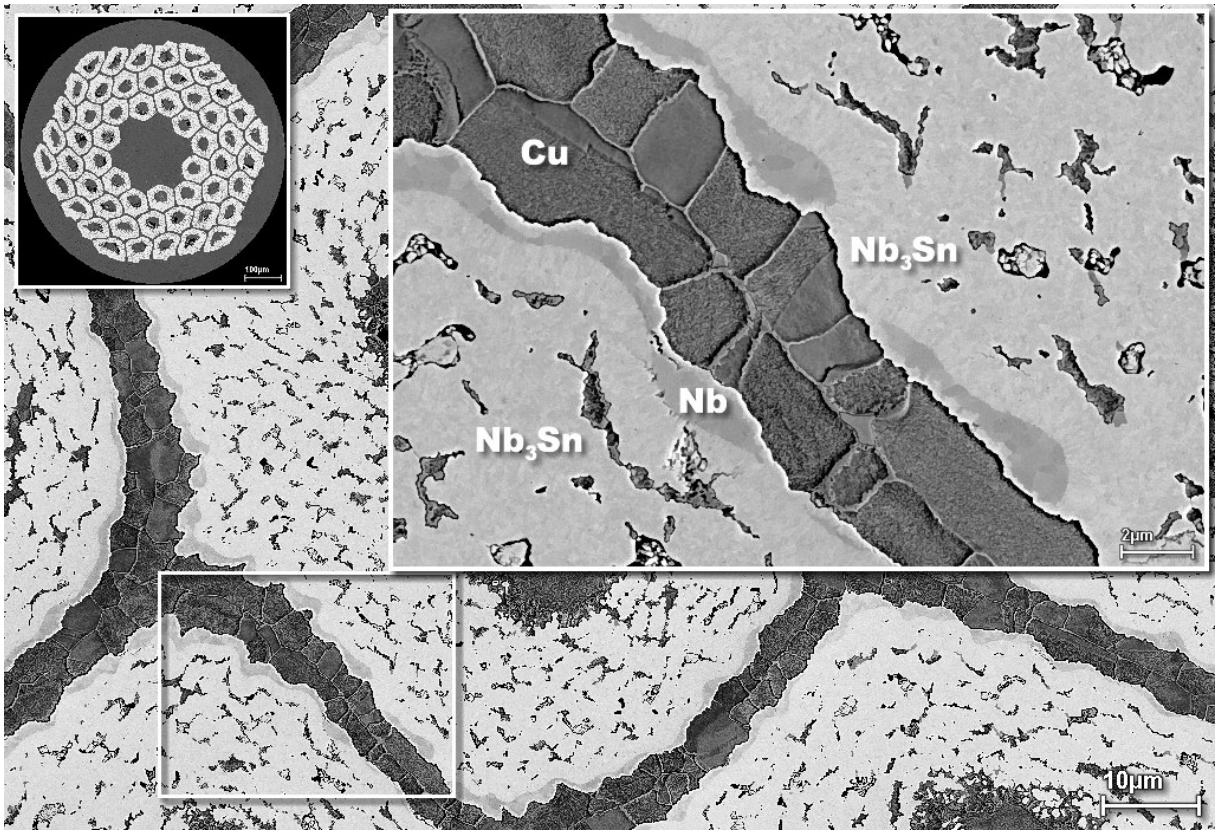

Fig. 7. BEI images of a high Sn MJR internal $Nb(Ti)_3Sn(Mg)$ strand manufactured by TWC. The Sn has reacted through the Nb diffusion barrier at some locations but as the etched detail reveals the Sn does not uniformly diffuse through the Cu stabilizer matrix but is mostly confined to the grain boundaries though which it diffuses to react the external Nb surfaces of adjacent sub-elements.

along the grain boundaries.

In high current Nb_3Sn strands of the type used to produce the 16 T dipole at LBNL [20], partial reaction of the Nb diffusion barriers is allowed, in fact the Nb_3Sn formed from the barrier makes an important contribution to the overall critical current density of the composite. In Fig. 7 we show a partial cross-section of such a strand and the reaction in the barrier can be seen to be complete at many points along the circumference of the sub-elements. Sn diffuses in the Cu stabilizer dropping the RRR of the strand, however the Sn is not uniformly distributed across the matrix; it diffuses along the Cu grain boundaries and reacts with the Nb diffusion barriers on adjacent sub-elements. The etching of the Cu matrix in Fig. 7 reveals the segregation of the Sn to the grain boundaries (confirmed by EDS microchemical analysis). Considering the final heat treatment of 675 °C is greater the half the melting point of the Cu, this is a surprising result. Typical of this type of high current internal Sn strand, the original filaments are no-longer separated and are part of a single layer of Nb_3Sn with each sub-element becoming a large single filament of Nb_3Sn with a shielded non-superconducting core consisting of the original Cu that has been surrounding the filaments combined with the original Sn that has been surrounding the Sn core.

Microstructural and Microchemical Homogeneity

There is interplay between microchemical homogeneity and microstructure in both Nb-47Ti

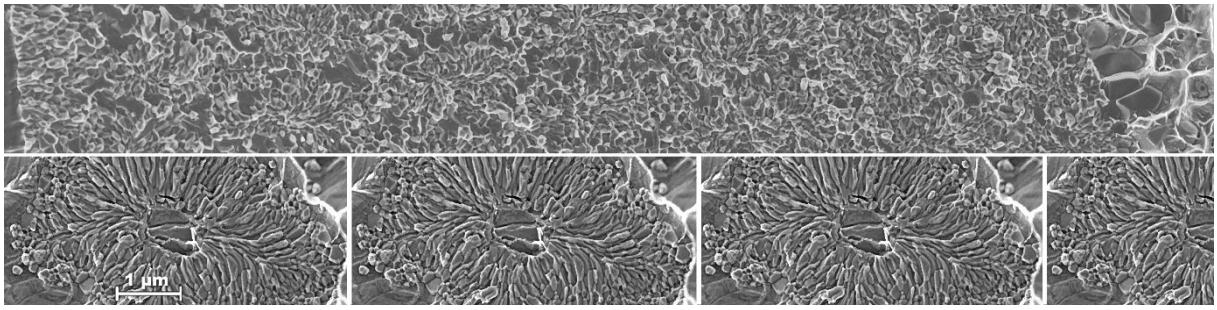

Fig. 8. High resolution in-lens secondary electron fractographs at the same magnification comparing the grain size and morphology of an entire Nb_3Sn layer from the OI-ST RRP strand used in the LBNL HD-1 16T Dipole with a bronze process filament (repeated) manufactured by VAC for the Benchmark 3 program of the ITER CSMC strand development program.

and Nb_3Sn: In Nb-47Ti both the morphology of α-Ti precipitate and the rate of precipitation of α-Ti very sensitive to composition. Under similar cold work conditions increased Ti content produces the Widmanstätten morphology of α-Ti which greatly increases the alloy hardness and reduces drawability. Decreasing the Ti content greatly reduces the volume of α-Ti precipitate. Thus microchemical inhomogeneity has both a macro-impact on the drawing stability of the strand and the local flux pinning force density. In Nb_3Sn reduced Sn supply results in a change in the Nb_3Sn grain morphology from equiaxed to columnar and also directly impacts the T_c and H_{c2} of the A15 phase. In Fig. 1 and 2 we have shown that there is even more to the issue of chemical homogeneity in Nb-Ti than was previously understood. In the bronze route filament shown in Fig. 5 we illustrate the well established transition for high-Sn equiaxed Nb_3Sn to Sn-poor columnar grains as grain growth continues into the core of the bronze filament with fewer and fewer new Nb_3Sn nucleated. The 3000 A/mm² (12 T, 4.2 K) Nb_3Sn conductors show very homogenous grain morphology across the entire A15 layer with columnar grain being observed only at the growing Nb-A15 interface.

Some of these characteristics are illustrated in Fig. 8 where we compare the grain size and morphology of an entire Nb_3Sn layer from the OI-ST RRP (Rod Restack Process) strand used in the LBNL HD-1 16T dipole with a bronze process filament (repeated) manufactured by VAC for the Benchmark 3 program of the ITER CSMC program. The average (log-normal) Nb_3Sn mean grain diameter for the VAC strand is 122 nm and that of the RRP strand is 110 nm. This difference is relatively small when one considers that the layer J_c of the ITER strand is 2250 A/mm² at 12 T and 4.2 K whereas the layer J_c of the RRP strand is ~5000 A/mm². The relative grain size and morphological homogeneity of the high-Sn-low-Cu RRP strand is evident from this image of the >3000 A/mm² (12 T, 4.2 K) strand. The variation in grain morphology in the strand has been shown to indicate compositional gradients across the layer[21]. In earlier 2000 A/mm² generation internal Sn strand with high Cu content the trend from equiaxed to more aspect grain morphology across the original filaments made it possible to observe the location of the original filaments[21]. In the new generation of high critical current density strands the trend is much smaller; however each original rod is marked by a layer of slightly larger grains. Is this perhaps a legacy of the Cu-Nb mechanical intermixing.

Conclusions

The improved resolution of scanning electron microscopes provides a new view to both established and developing fabrications routes for Nb-47Ti and Nb_3Sn. In both cases the microchemical in inhomogeneity can be shown for all the components at the same time down

to a sub 20 nm scale. Comparing low-hysteresis loss high Cu:Sn ratio Nb_3Sn strands with high J_c low Cu:Sn ratio strands we show that average grain size can be similar but layer critical current increases by a factor of two in the low-Cu case. The sensitivity of critical current density to Nb_3Sn composition is clearly much greater than was previously assumed.

Acknowledgements

We would like to thank Seung Hong, Mike Field and Jeff Parrell of OI-ST, Eric Gregory and Bruce Zeitlin of Supergenics, Hem Kanithi of IGC-AS (now Outokumpu Advanced Superconductors), Manfred Thoener of VAC (now European Advanced Superconductors) and Paul Jablonski (now at DOE-Albany) and Jim McKinnell (now at Hewlett Packard) of TWC and for the strands supplied for this work. The strand heat treated with the 16 T dipole was supplied by Ron Scanlan of LBNL. Metallographic assistance was supervised by Bill Starch at the UW. The work was supported through the U.S. Department of Energy, by both the Department of High Energy Physics under Grant DE-FG02-91ER40643 and the Office of Fusion Energy Sciences under Grant DE-FG02-86ER52131

References

[1] J. K. Hulm and R. D. Blaugher, Phys. Rev. 123:5 (1961) 1569.
[2] J. E. Kunzler, E. Buehler, F. S. L. Hsu, and J. H. Wernick, Phys. Rev Lett. 6:3 (1961) 89.
[3] E. W. Howlett, Great Britain Patent 52,623/69 (1969).
[4] A. R. Kaufman and J. J. Pickett, Bull. Am. Phys. Soc., 15, (1970) 833.
[5] K. Tachikawa, Proc. 3rd Int. Cryogen. Eng. Conf. (ICEC3), Berlin, (1970), 339.
[6] K. Tachikawa and Y. Iwasa, Appl. Phys. Letters, 16:6 (1970) 230.
[7] Zhang Tingjie, Wang Keguang, Wu Xjaozu, Li Chengren and Zhou Nong, Proc. Tenth Int. Cryogenic Engineering Conf. (ICEC10) ed H Collan, P Berglund and M Krusius, (1984), 700.
[8] O. V. Chernyi, N. F. Adrievskaya, V. O. Ilicheva, G. E. Storozhilov, P. J. Lee, and A. A. Squitieri, Advances in Cryogenic Engineering, 48:B (2002) 883.
[9] Motowidlo, R., Rudziak, M. K., Wong, T., IEEE Trans. Applied Superconductivity, 13, (2003) 3351.
[10] P. J. Lee and D. C. Larbalestier, to be published in IEEE Proc. 2003 Particle Accelerator Conference.
[11] P. J. Lee, C. D. Hawes, M. T. Naus, A. A. Squitieri, D. C. Larbalestier, IEEE Transactions on Applied Superconductivity, 11(1), (2001) 3671.
[12] H. H. Farrell, G. H. Gilmar, and M. Suenaga, J. Appl. Phys., 45 (1971), 4025.
[13] K. Togano, Y. Asano, and K. Tachikawa, J. Less Common Metals, 68 (1979), 15.
[14] P. J. Lee, C. M. Fischer, W. Gabr-Rayan, D. C. Larbalestier, M. T. Naus, A. A. Squitieri, and W. L. Starch, E. Z. A. Barzi, P. J. Limon, G. Sabbi, and A. Zlobin, H. Kanithi, S. Hong, J. C. McKinnell and D. Neff, Trans. Applied Superconductivity, 9:2 (1999) 1559.
[15] K. Faase, P. Lee, J. McKinnell, and D. Larbalestier, Advances in Cryogenic Engineering (Materials), 38 (1992) 723.
[16] B. G. Lazarev, V. A. Ksenofontov, I. M. Mikhailovskii, O. A. Velikod-naya, Low Temperature Physics, 24:3 (1998) 205.
[17] P. J. Lee, J. C. McKinnell, and D. C. Larbalestier, Adv. Cryo. Eng. (Materials), (1990) 287.
[18] M. Suenaga and W. Jansen, Appl. Phys. Lett., 42 (1983) 791.
[19] Bruce A. Zeitlin, Eric Gregory, Taeyoung Pyon, R. M. Scanlan, Anatolii A. Polyanskii, and Peter J. Lee, Paper M1-D-08 Presented at CEC-ICMC 2003, to be published in Adv. Cryo. Eng. (2004).
[20] S. Gourlay, S. Bartlett, P. Bish, S. Caspi, L. Chiesa, D. Dietderich, P. Ferracin, R. Hafalia, H. Higley, A. Lietezke, N. Liggins, A. McInturff, "Test Results for HD-1, a 16 Tesla Block-Dipole Magnet" Paper 4AA03 presented at MT-18, October 2003, to be published in IEEE Trans. MAG. (2004).
[21] P. J. Lee, C. D. Hawes, M. T. Naus, A. A. Squitieri, D. C. Larbalestier, IEEE Transactions on Applied Superconductivity, 11:1 (2001) 3671.